nature astronomy

Article

https://doi.org/10.1038/s41550-026-02931-5

Evidence of a massive accretion event 1.8 billion years before the Gaia-Sausage-Enceladus merger

Received: 26 January 2026

Accepted: 23 June 2026

Published online: 17 August 2026

Check for updates

Davide Massari [1] ✉, Chiara Zerbinati [1,2], Cristiano Fanelli [1], Amina Helmi [3], Edoardo Ceccarelli [1,2,3], Fernando Aguado-Agelet [4,5], Santi Cassisi [6,7], Ewoud Wempe [3,8], Matteo Monelli [6,9], Andrea Bellini [10], Thomas M. Callingham [3,11], Hanneke C. Woudenberg [3], Roger E. Cohen [12], Carme Gallart [13], Elena Pancino [14], Sara Saracino [14], Maurizio Salaris [1,15] & Alessio Mucciarelli [2]

The merger history of the Galaxy has been traced back firmly to a redshift of 2 (10 billion years ago). While evidence for the existence of at least one more substantial merger before this time has been presented, its interpretation is yet to be fully established. Here we show that the population of globular clusters around the Galaxy depicts three distinct age–metallicity sequences, one associated with the progenitor of the Milky Way, one with the merger with Gaia-Sausage-Enceladus 10 billion years ago and a third intermediate sequence associated with at least one merger that we estimate took place about 1.8 billion years before Gaia-Sausage-Enceladus. This discovery has been possible thanks to exquisite Hubble Space Telescope data and sophisticated analysis that enables very precise relative age determination of globular clusters. The newly identified sequence reveals that this merger took place with an object of a similar stellar mass to that of Gaia-Sausage-Enceladus ($\simeq 5 \times 10^8$ stellar masses, $M_{\odot}$) that deposited most of its mass in the inner 6 kpc of the Milky Way. The identification of a third merger event in the inner Galaxy puts to rest earlier debates and, honouring previous works, we name the progenitor system Low-energy-Kraken-Heracles, or LKH for short.

According to the currently favoured cosmological framework, large galaxies like the Milky Way have grown through time, at least in part, via mergers with smaller systems. Our knowledge of the history of events that contributed to the assembly of our Galaxy has greatly improved[1] thanks to the advent of the Gaia mission[2] and large spectroscopic surveys (for example, Apache Point Observatory Galactic Evolution Experiment (APOGEE)[3], Galactic Archaeology with HERMES (GALAH)[4]). The most recent merger, still ongoing, is the one with the Sagittarius dwarf galaxy[5], which fell in about 6 billion years (Gyr) ago[6]. Before this, the most massive merger known to be experienced by the Milky Way was with the Gaia-Sausage-Enceladus (GSE) dwarf galaxy[7,8], which ended about 10 Gyr ago[9,10]. Owing to the high mass ratio of this event (about 1:4 to 1:5), this led to the development of the thick disk as we see it today, both through dynamical heating and enhanced star formation[9,11,12]. A few other accretion events have also taken place between these two important mergers (that is, between 6 and 10 Gyr ago), all involving smaller dwarf galaxies[13–15].

Reconstructing what happened in the earliest phases of the Milky Way's life, more than 10 Gyr ago, is definitely more challenging. As we proceed backwards in time, the mass of our Galaxy must have been smaller and more comparable to that of the accreting building blocks[16]. As a result of this and the extremely short evolutionary timescales,

A full list of affiliations appears at the end of the paper. ✉e-mail: davide.massari@inaf.it

https://doi.org/10.1038/s41550-026-02931-5

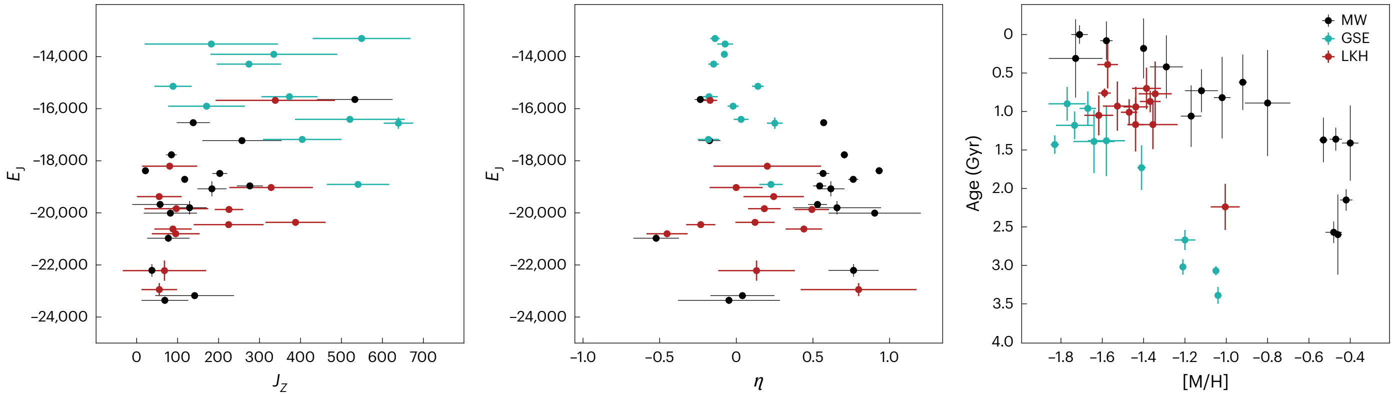

Fig. 1 | Chrono-dynamical properties of our sample of 39 GCs. Left: distribution in the E_J versus J_Z dynamical space of the 39 GCs with homogeneous age estimate (filled symbols; Methods). GCs are colour-coded according to their association (with membership probability >50%) with GSE, the Milky Way (MW) or the LKH as determined by our Bayesian chrono-dynamical analysis. Uncertainties are derived as the 16th and 84th percentiles of each parameter distribution computed over 200 orbits. Middle: corresponding distribution in the E_J vs η space. Uncertainties are computed in the same way. Right: distribution in the age–metallicity plane. The relative age scale along the y axis is defined by setting the age resulting from the isochrone fit of the oldest GC (t_{iso} = 14.48 Gyr) as zero. Uncertainties on age and [M/H] are computed as described in detail in ref. 34. The legend in the right panel applies to all panels.

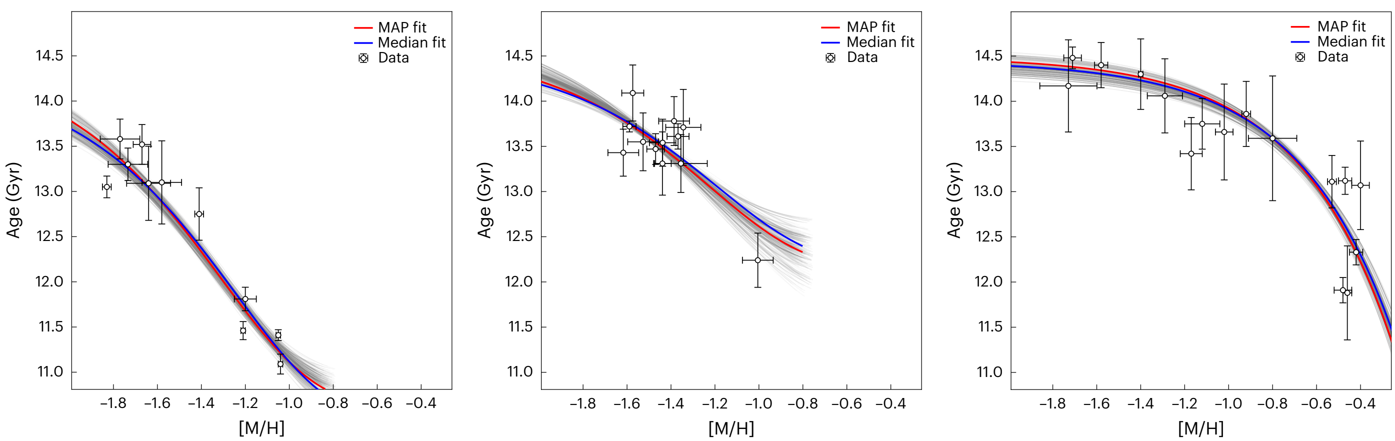

Fig. 2 | AMR model fits. Left: fit to the GSE GCs. Middle: fit to the LKH GCs. Right: fit to the in situ Milky Way GCs. The individual GC members of the three samples are selected as described in Methods. Error bars are as in the right-hand panel of Fig. 1. The red line corresponds to the fit with the maximum a posteriori (MAP) value, while the blue line represents the median fit. The grey curves show the 500 individual models with the highest posterior probability from the MCMC run.

the properties of the infant Milky Way and those of the merging systems could be difficult to distinguish either dynamically or chemically[17–19]. The very short mixing timescales (driven in part by chaos in the inner Galaxy induced by the rotating bar) imply that some of the dynamical memory must have been erased[20]. Furthermore, because of the intricacies of modelling chemical evolution, state-of-the-art cosmological hydrodynamical simulations currently provide limited guidance on all of the chemical elements that could potentially be used to distinguish the early building blocks from one another[17,19].

The current understanding is that the earliest phases of the Milky Way evolution are represented by dynamically hot[21,22], chemically unevolved[23,24] stellar populations, concentrated in the inner 3 kpc of the present-day Galaxy[25]. These populations are probably a mix of stars born in the main progenitor (in situ) and of stars born in building blocks accreted early on, but the dispute over their origin is not settled yet. Attempts to observationally isolate the in situ population from the accreted building blocks have yielded debated results so far, with cross-contamination being the major challenge. Using a compilation of literature age estimates, a group of globular clusters (GCs) with low orbital energy (hereafter the Low-energy group), concentrated within 6 kpc of the Galactic centre, was identified and presumed to be related to an accretion event[26]. Subsequently, these GCs were interpreted as being associated with the Kraken merger event[27], an entity that had been predicted[28] using cosmological numerical simulations on the basis of the number of GCs with unknown origin along the branch of the age–metallicity relation (AMR) populated by accreted systems. However, the accreted origin of these GCs has been contested on the basis of chemo-dynamical arguments[29,30]. Similarly, the search for accreted stars in the inner Galaxy led to the identification of a metal-poor and chemically unevolved population, which was named Heracles[31]. However, its origin is also debated[21,32], as the stars' chemical properties are not exclusive of accreted populations and may be found in early in situ populations as well (at least in the elements considered thus far and in the metal-poor regime). A more recent analysis[24] that also considered the spatial distribution of the Heracles stars nonetheless seems to provide further support for the presence of an accreted population.

The difficulty of differentiating the in situ population from that accreted in the earliest phases of the Milky Way evolution[24,33] suggests that more information is needed. Crucially, chronological information can be used to sequence the events that took place in the proto-Galaxy. While relative ages are difficult to determine accurately and precisely for individual stars, it is possible to do so for star clusters[34,35].

Here we homogeneously analyse a sample of 17 GCs in the inner Galaxy, where the debris of the earliest accretion events should be

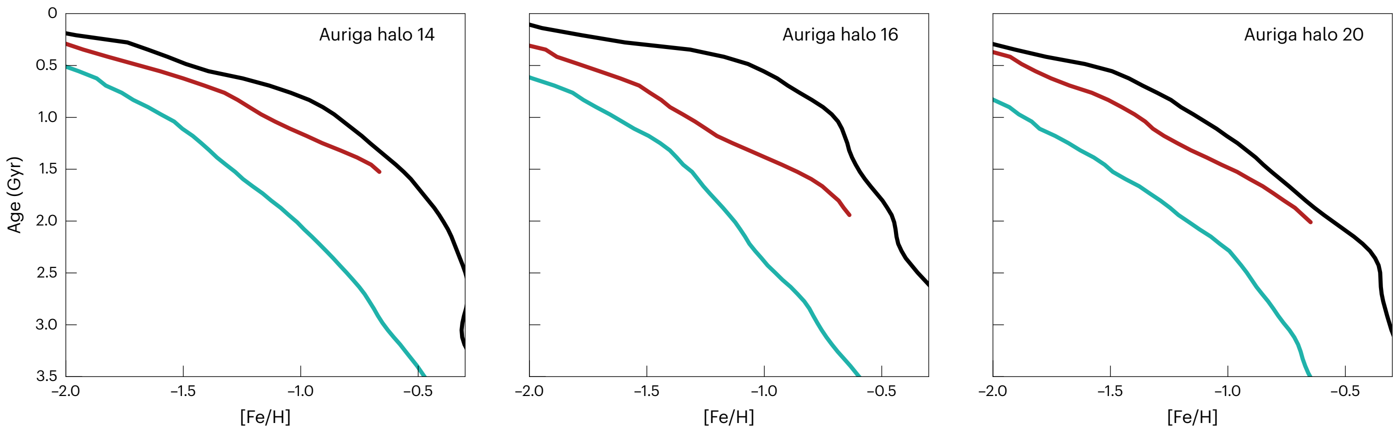

Fig. 3 | AMR in simulated Milky Way analogues. Median trends (solid lines) for the AMR of the main progenitor (black), a GSE-like merger (cyan) and an LKH-like event (red) in three Milky Way analogues of the Auriga Level-4 simulations are shown. Left: Auriga halo 14. Middle: Auriga halo 16. Right: Auriga halo 20.

located[36]. These GCs have been observed with the Hubble Space Telescope (HST) in the F606W and F814W optical bands, and 15 of these have been dynamically associated with the Low-energy group in previous works[26,37]. Using our recently developed highly sophisticated analysis, we are able to determine extremely precise relative GC ages with typical errors of a few hundred million years[34] (see 'Age estimates' in Methods for details). The increase in precision is due to the minimization of systematic errors, driven in previous works by the heterogeneity of datasets and methodologies, as well as a more sophisticated treatment of each cluster's photometry.

With our analysis of these 17 GCs, this brings the total number of GCs with homogeneous age determinations to 39 (refs. 34,38–40). Besides the Low-energy group, we expect[41] this sample to also contain in situ GCs and some associated with GSE. To robustly determine the most likely number of progenitors required to describe this chrono-dynamical dataset, we fitted a Bayesian model with multiple components (each representing a progenitor system) using the dynamic nested-sampling package dynesty (version 3.0.0)[42]. We assumed that each progenitor follows an AMR, described using a simple chemical evolution model[43] (see 'AMR models' in Methods for details). We also assumed that the associated GCs are clustered in terms of their Jacobi energy (E_J), (average) vertical action J_z and (average) circularity $\eta = L_z/L_z(E)$, where L_z is the vertical angular momentum and E is energy (see Methods for a justification of this choice of dynamical quantities). To compute these, we used a Galactic mass model that included a rotating bar[20,44] and computed the averages over 200 orbits. The distribution of clusters was taken as a mixture of K Student's t-distributions, where K is to be determined, and corresponded to the number of progenitors. This statistical approach allowed us to identify distinct chrono-dynamical groups while properly accounting for observational uncertainties and model evidence. By adopting flat priors on the characteristic parameters of the AMR, we estimated the Bayesian evidence (log$Z$) for different cases with $K = 2$, 3 and 4 separate progenitors. We found that the case with the strongest evidence was the one with three progenitors. In comparison to it, the two-progenitor case has $\Delta \log Z = 5.3$, and is therefore decisively disfavoured according to both the scales by Jeffreys[45] and by Kass and Raftery[46]. The four-progenitor case instead has $\Delta \log Z = 2.2$, and is thus strongly and moderately disfavoured, respectively, according to the two scales.

Figure 1 shows the distribution of the 39 GCs in our sample in dynamical space (left and middle) and in the age–metallicity plane (right panel), colour-coded by their membership as determined by our statistical analysis in the most favoured case with three components. It is immediately evident that there is an intermediate population of GCs (red symbols) that follows an age–metallicity sequence that is well separated from that traced by GSE GCs (cyan symbols) and the in situ GCs (black symbols). These 12 GCs (out of the 15 in our sample initially associated with the Low-energy group) are confined within 6 kpc of the Galactic centre. Hence, most of the 'low-energy' GCs must have formed in an environment that is neither GSE nor the Milky Way and, given their distinct dynamical properties, it follows that this population of GCs is necessarily part of an independent merger event.

While the above statistical analysis allows us to identify the presence of three distinct populations of GCs (see 'Statistical analysis and characterization of the progenitors' in Methods for details), to more accurately constrain the properties of their progenitor systems we fitted the AMR of the three groups separately, using the GCs with a high-probability ($p > 50\%$) of membership. As before, we used a simple chemical evolution model[43], with parameters depending on the stellar mass of a galaxy[47], the time at which star formation started and the time at which it ended, which we took to represent the galaxy's accretion time (see Methods for details). Figure 2 shows the individual fits of the three AMRs. From the comparison between GSE GCs and the intermediate population of GCs, we find that the merger event identified here has a stellar mass consistent with that of GSE within the uncertainties. Moreover, its accretion time is ~1.8 Gyr earlier than GSE. These relative measurements are robust, and are anchored to absolute values by taking a stellar mass of ~5×10^8 solar masses ($M_\odot$) and an accretion time of $t_{accr} \simeq 10.5$ Gyr (ref. 48) as a reference for GSE[7].

It follows that we have identified a very significant merger event that took place ≃12.3 Gyr ago (at redshift $z > 4$) with a mass ratio that must have been higher than that of the GSE event[7,9] (that is, >0.2–0.3). The estimated stellar mass for these two progenitors is in agreement with the host stellar mass–GC metallicity relation[49], according to which a galaxy this massive (with an absolute magnitude in the B band[50] of $M_B \simeq -17.5$) should host a GC system of mean metallicity [M/H] ≃ −1.4.

This early and massive merger has characteristics that could link it to the putative accreted Heracles stellar population, which is also restricted to the inner Galaxy[31]. While this region of the Galaxy probably contains debris from all of the mergers that took place in the early stages of formation of the Milky Way, our identification may be seen as a clean selection extending to low metallicity of the most massive contributor to the Heracles' accreted sub-population. Nonetheless, we cannot rule out the presence of other (presumably less massive) progenitors without GCs or progenitors whose GCs have been fully disrupted. As the members of this progenitor stem mostly from the Low-energy group[26], later associated with the putative Kraken[27], we name the progenitor Low-energy-Kraken-Heracles (LKH).

This identification of a massive event that occurred during the early evolution of the proto-Galaxy from the intricate sequence of mergers and in situ star formation thus settles the debates mentioned earlier. Moreover, our study establishes the AMR as a tracer that is able to distinguish the main progenitor of our Galaxy, namely the building block that evolved at the highest rate, in the metal-poor regime ([Fe/H] $\lesssim -1.6$).

Our conclusions are strongly supported by cosmological simulations, which typically predict between one and four substantial mergers in the history of a Milky Way-like galaxy[51]. Furthermore, the three AMRs identified in our work are in fact remarkably well reproduced by several Milky Way analogues of the Auriga simulations[52], as shown in Fig. 3. In the three simulated galaxies represented in Fig. 3 (Au14, Au16 and Au20), the median AMRs defined by the stars are shown for the main progenitor, a GSE-like merger (defined as the largest accretion event that occurred between 2.5 Gyr and 5 Gyr from the start of the simulation) and an LKH-like event (defined as the largest event within the first 2.5 Gyr). The AMRs in the simulations follow a global trend that is in good agreement with observations, in particular showing a clear separation among the AMRs of the three progenitors of a few hundred million years at any metallicity, which qualitatively matches the separation observed with the GCs analysed in this article. Future precise stellar ages for large samples of stars in the inner Milky Way, particularly measurements from asteroseismology missions such as PLAnetary Transits and Oscillations of stars (PLATO)[53] or those derived with CMD-fitting techniques using Gaia data, will be key to unravel the series of events that took place in the first billion years of the Milky Way's life in even greater detail.

Methods

Age estimates

The relative ages of all of the clusters analysed in this work were determined with the strictly homogeneous method developed within the Cluster Ages to Reconstruct the Milky Way Assembly (CARMA) project[34,38,39,54]. All of the details have been extensively described in paper I of the series[34]. Here we remark that the precision that we achieve is due to the minimization of the sources of systematic errors, which in turn is achieved through the adoption, for all of the CARMA GCs, of: (1) homogeneous HST photometry in the F606W and F814W bands, corrected for differential reddening[55] and decontaminated from field stars via proper-motion-based membership[56]; (2) the most up-to-date stellar evolution models from the Bag of Stellar Tracks and Isochrones (BaSTI) database[57,58] and (3) the same Markov chain Monte Carlo (MCMC)-based isochrone fitting technique, which provides estimates of the age, global metallicity [M/H], distance and colour excess $E(B-V)$, all on the same homogeneous scale. We note that our age estimates should not be interpreted on an absolute scale, because it is well known that every set of theoretical models has a different absolute scale based on the adopted input physics. In this sense, GC ages older than the age of the Universe should not raise concern. They should be interpreted bearing in mind that they could be inaccurate, but highly precise, which is what is important for all of the results presented here.

We determined age estimates in the CARMA framework for 17 GCs, namely: 15 originally associated with the Low-energy group and 2 dynamically interpreted as in situ. The photometry for most of these GCs comes from the public database of the HUGS project[56,59]. The astro-photometric catalogues of NGC 6256, NGC 6401 and NGC 6453 are from another source[60]. Finally, the photometry of NGC 4372 was obtained with the same codes and methods used for the other GCs[61] by working on images from GO-15982 (PI, M. Reinhart).

The result of the isochrone fit is summarized in Supplementary Table 1. An example of an individual fit is presented in Supplementary Fig. 1. As a sanity check, we compared the values of the free parameters that we obtained from the isochrone fit with existing literature estimates. The comparison is shown in Supplementary Fig. 2, and demonstrates that the mean difference (solid grey lines) is always consistent with zero within 1σ (dashed grey lines). Literature colour excesses $E(B-V)_{ref}$ and distance moduli DM_{ref} are from the Harris catalogue[62], but the same good consistency is found when considering distance estimates from other works[63]. The global metallicity $[M/H]_{ref}$ was computed starting from the [Fe/H] values of the Harris catalogue, and transformed according to the equation[64] $[M/H] = [Fe/H] + \log(0.694 \times 10^{[\alpha/Fe]} + 0.306)$, where $[\alpha/Fe]$ indicates the alpha-element abundance ratio, and using a relation[38] between [Fe/H] and $[\alpha/Fe]$.

Important effort has been devoted to the determination of the relative ages of Milky Way GCs in the past[65,66]. To compare the uncertainty in our age estimates with previous works, we used the samples by Dotter et al.[67] and by VandenBerg et al.[35], as they determined GC relative ages using the photometry in the same F606W and F814W HST filters adopted here. Given that the precision of the GC age depends on GC properties such as distance or reddening, we only compared GCs in common with the two works. Of the 17 GCs for which we provide a CARMA age, 12 are in common with the Dotter sample and 12 (not strictly the same ones) with the VandenBerg sample. Our uncertainties are on average a factor of 3.5 better than the former (a mean error of 0.26 Gyr versus 0.91 Gyr) and a factor 1.6 better than the latter (a mean of 0.26 Gyr versus a mean of 0.43 Gyr). While some of the sources of errors affecting our estimates and those in these works should in principle be similar, the most notable differences are the following: (1) our CMDs were always corrected for differential reddening and decontaminated from field stars using proper motions measurements; (2) when a particular GCs is known to host stellar populations enriched in iron, helium (Y) or C + N + O (which also affect the photometry in optical bands, contrarily to the standard multiple population phenomenon), we removed the chemically peculiar stars using HST UV photometry; (3) we corrected our theoretical models for temperature-dependent extinction; (4) we did not fix the GC metallicity, distance or reddening, but instead left them as free parameters in the fit.

AMR models

The simple chemical evolution model[43] enables an AMR to be inferred under relatively straightforward assumptions. For a constant star-formation rate (SFR), the age t is related to the metallicity as:

$$t(x) = t_f + \Delta t \times \exp\left[-\frac{10^x}{p}\right] \quad (1)$$

where x = [M/H] is the metallicity, p is the effective chemical yield (in units of $Z_\odot$) and $\Delta t = t_i - t_f$ denotes that star formation started t_i billion years ago and ended after a time interval $t_i - t_f$, where $t_i > t_f$. In the case of an exponentially declining SFR (that is, $\propto\exp(-\beta t)$, where β is the coefficient of the exponential function), the age and metallicity are related through:

$$t(x) = t_i - 10^x/(\beta p) \quad (2)$$

when the star-formation timescale is much longer (that is $t_i \gg t_f$). In the opposite case, it can be shown that equation (2) reduces to equation (1). For the Milky Way, which is the progenitor that endured star formation the longest, we adopted an exponentially declining SFR, hence equation (2). For the accreted systems, as both β and t are small, we adopted equation (1). We remark that in our analysis we adopted t_f as the indicator for the merger accretion time. Although such an assumption is not novel[27], it has been shown that a delay of 0.5–1.5 Gyr might occur between the end of GC formation and the conclusion of an accretion event[68]. However, this does not affect our reconstructed merger timeline, as it relies on the relative comparison between the t_f values inferred for each different progenitor.

We assumed the effective chemical yield p to be constant over time and to be proportional to the stellar mass of the progenitor[47] according to the relation[43]:

https://doi.org/10.1038/s41550-026-02931-5

$$p = 0.005\left(\frac{M}{10^6 M_\odot}\right)^{0.4}. \quad (3)$$

The value of the coefficient in equation (3) was determined to better represent the yield of the progenitor systems of the Milky Way, where type Ia supernovae did not have the time to contribute significantly[43]. As such, it is a factor of 2 smaller than the original value describing present-day dwarf galaxies[47].

Statistical analysis and characterization of the progenitors

As described in the main text, we determined the most likely number of progenitors in our dataset using chrono-dynamical information[37] and employing the dynamic nested-sampling package dynesty. This is done through a stepwise procedure as follows:

(1) To anchor the AMR of the in situ and GSE progenitors, we first selected a few clusters with homogeneous chemo-chrono-dynamical properties that in the literature are consistently and unambiguously associated with either of these progenitors. We assigned NGC 5927, NGC 6304, NGC 6352, NGC 6388, NGC 6441 and NGC 6496 (according to previous work[34,69]) and NGC 6218, NGC 288, ESO452-11 and NGC 6362 (based on previous analysis[39]) to the in situ component, whereas NGC 362 and NGC 1261 were assigned to the GSE component[39].

(2) We assumed that each of the multiple components/progenitors follows an AMR and is clustered in the dynamical space described by the separable parameters (E_J, J_Z, η). E_J is preferred to the more often used E, because the latter is not an integral of motion for many of the clusters in our sample because of the Galactic bar. Furthermore, we preferred to replace the traditional L_z with η because E_J is already related to L_z ($E_J = E - \Omega_b L_z$, where Ω_b is the bar rotation speed) and η contains information on both the eccentricity of the orbit and its sense of rotation. Finally, J_z is sensitive to complementary information (as is the angular momentum perpendicular to the vertical one, $L_\perp$) on an orbit, such as to vertical position and velocity, and although (like η) it is not fully conserved, it is an action and we do account for its variation in our analysis.

Concerning the AMR, we used flat priors on the progenitor mass $M_\star$, t_i, t_f and (whenever necessary) β, enforcing the constraint $t_i - t_f > 1$ Gyr. We did not sample the yield parameter p directly but instead obtained it from $M_\star$ using equation (3), which therefore implies a non-flat prior on p. Each of the dynamical parameters was modelled as a one-dimensional Student's t likelihood (with a number of degrees of freedom $\nu = 4$) centred on the mean value of each component, and with a scale given by the sum in quadrature of the measurement uncertainties and the intrinsic dispersion. Clustering was implemented directly in the total likelihood through a K-component mixture.

(3) We computed the Bayesian evidence for the cases with two, three and four components.

We found that the most likely case is the one that includes three progenitors. We tested that this result is robust to the choice of the GCs anchored in step (1). In fact, by reducing these to the six most metal-rich ones, the Bayesian evidence continues to favour $K = 3$ over $K = 2$ decisively ($\Delta\log Z = 12.9$) and over $K = 4$ more moderately ($\Delta\log Z = 2.1$). At the same time, our Bayesian mixture analysis provided the values for the AMR parameters, as well as the posterior membership probabilities for each component. This allowed us to define the samples of GCs belonging to each progenitor as those with a membership probability of >50%:

- in situ component: other than those assigned initially, the analysis added NGC 4372, NGC 6205, NGC 6397, NGC 6401, NGC 6656 and NGC 6752
- GSE component: already included NGC 362 and NGC 1261, further encompasses NGC 1851, NGC 2298, NGC 2808, NGC 6341, NGC 5897, NGC 6779, NGC 6809, NGC 7089 and NGC 7099;
- LKH component: NGC 4833, NGC 5286, NGC 5986, NGC 6093, NGC 6121, NGC 6144, NGC 6254, NGC 6256, NGC 6453, NGC 6535, NGC 6541 and NGC 6681

We note that there is significant overlap between the original Low-energy group and LKH, as 91% of its GCs (10 out of 11) are in common[41]. Moreover, we tested that these associations are robust to the inclusion of a small (200-Myr) intrinsic spread of the individual AMRs. Additional or improved age measurements might cause some GC associations to change, especially those of the GCs that are at the boundaries of the three populations in the chrono-dynamical space. Using bootstrapping, we have, however, tested that the existence of the three AMR sequences is robust to such changes, as is the derivation of their properties.

We used this list of likely members of each progenitor to characterize these better. Although our Bayesian mixture model had fitted AMRs, it used all clusters simultaneously and hence provides less strict constraints on their properties. Therefore, to characterize each progenitor in terms of $M_\star$ (through p) and t_i, we MCMC fitted each individual AMR using priors informed by the 5D nested-sampling posterior. For $M_\star$ we adopted lognormal priors, whereas for t_i, t_f and (whenever applicable) β, we used wide, flat priors. Specifically, for the mass of GSE we adopted $\ln M_\star \sim \mathcal{N}(\mu, \sigma^2)$ with (μ, σ) = (20, 1), corresponding to a median $M_\star \approx 5\times10^8\,M_\odot$ and a 1σ scatter of almost a factor of three around the median. For LKH we assumed the same prior, motivated by the 5D nested-sampling posterior, which favours a mass of a similar order of magnitude. The star-formation times t_i and t_f were regulated by uniform priors within fixed bounds. In particular, we used $t_i \in [t_{i,\min}, t_{f,\max}]$ and $t_f \in [t_{f,\min}, t_{f,\max}]$, with $(t_{i,\min}, t_{f,\min}, t_{f,\max}) = (8, 8, 15)$ Gyr. When sampled (linear AMR), β was assigned a wide uniform prior within fixed bounds ∈[0.01, 2.00]. The likelihood function was assumed to be Gaussian in both metallicity and age, and defined as:

$$\ln\mathcal{L} = \sum_{n=1}^{N} \ln\mathcal{N}\left(z_n^{\rm obs}|z_n^{\rm true}, \sigma_{z,n}^2\right) + \sum_{n=1}^{N} \ln\mathcal{N}\left(t_n^{\rm obs}|t_n^{\rm model}, \sigma_{t,n}^2 + \sigma_{\rm int}^2\right) \quad (4)$$

where $z_n^{\rm obs}$ and $t_n^{\rm obs}$ are the observed metallicities and ages, with measurement uncertainties $\sigma_{z,n}$ and $\sigma_{t,n}$, respectively, and $z_n^{\rm true}$ are latent 'true' metallicities sampled in the MCMC. The model prediction $t_n^{\rm model}$ is given by the adopted AMR parametrization evaluated at $z_n^{\rm true}$ and parameters (p, t_i, t_f) (or (p, t_i, β) for the exponentially decaying SFR form). Here $\ln\mathcal{N}(x|\mu, \sigma^2)$ denotes the full Gaussian log density. The age variance includes an additional intrinsic-scatter term, added in quadrature to the observational uncertainty, for which we adopted a weakly informative prior.

For each dataset we ran an MCMC sampler with $n_{\rm walkers} = 128$, performing $n_{\rm steps} = 20{,}000$ iterations and discarding the first 25% as burn-in. We initialized all walkers with scattered starting points to ensure broad coverage of the parameter space. The mass scaling parameter of each walker was set by uniformly drawing a test mass along its previous range and mapping it to p, whereas t_i and t_f were offset from their lower bounds by small Gaussian perturbations. We assessed the MCMC convergence using the Gelman–Rubin ($\hat{R}$) diagnostic, effective sample size (ESS) and autocorrelation analysis. All of the parameters yielded $\hat{R}$ values <1.01, ESS > 10^6 and first-lag autocorrelation ≤|0.04|, proving good chain mixing and highly efficient sampling.

The results of the AMR model fit are summarized in Supplementary Table 2, and interpreted in the main text. The corresponding corner plots are shown in Supplementary Figs. 3–5.

Data availability

Most of the GC photometric catalogues analysed here are available through the HUGS project portal at https://archive.stsci.edu/prepds/

hugs. Those that are not present in that repository are available upon request from the corresponding author or R.E.C. (rc1273@physics.rutgers.edu). GC age estimates and dynamical associations are available at https://www.oas.inaf.it/en/research/m2-en/carma-en.

Code availability

The code employed to perform the statistical analysis and to fit the AMRs with theoretical models is provided in Supplementary Code 1. The code used to perform the isochrone fit has been developed in the context of the CARMA[34] and Hubble-Missing Globular Cluster Survey[40] projects, and will be released at the projects conclusion. Interested readers should contact the corresponding author.

References

1. Helmi, A. Streams, substructures, and the early history of the Milky Way. *Annu. Rev. Astron. Astrophys.* **58**, 205–256 (2020).
2. Gaia Collaboration et al. The Gaia mission. *Astron. Astrophys.* **595**, A1 (2016).
3. Majewski, S. R. et al. The Apache Point Observatory Galactic Evolution Experiment (APOGEE). *Astron. J.* **154**, 94 (2017).
4. Buder, S. et al. The GALAH+ survey: third data release. *Mon. Not. R. Astron. Soc.* **506**, 150–201 (2021).
5. Ibata, R. A., Gilmore, G. & Irwin, M. J. A dwarf satellite galaxy in Sagittarius. *Nature* **370**, 194–196 (1994).
6. Ruiz-Lara, T., Gallart, C., Bernard, E. J. & Cassisi, S. The recurrent impact of the Sagittarius dwarf on the star formation history of the Milky Way. *Nat. Astron.* **4**, 965–973 (2020).
7. Helmi, A. et al. The merger that led to the formation of the Milky Way's inner stellar halo and thick disk. *Nature* **563**, 85–88 (2018).
8. Belokurov, V., Erkal, D., Evans, N. W., Koposov, S. E. & Deason, A. J. Co-formation of the disc and the stellar halo. *Mon. Not. R. Astron. Soc.* **478**, 611–619 (2018).
9. Gallart, C. et al. Uncovering the birth of the Milky Way through accurate stellar ages with Gaia. *Nat. Astron.* **3**, 932–939 (2019).
10. Montalbán, J. et al. Chronologically dating the early assembly of the Milky Way. *Nat. Astron.* **5**, 640–647 (2021).
11. Di Matteo, P. et al. The Milky Way has no in-situ halo other than the heated thick disc. Composition of the stellar halo and age-dating the last significant merger with Gaia DR2 and APOGEE. *Astron. Astrophys.* **632**, A4 (2019).
12. Belokurov, V. et al. The biggest splash. *Mon. Not. R. Astron. Soc.* **494**, 3880–3898 (2020).
13. Myeong, G. C., Vasiliev, E., Iorio, G., Evans, N. W. & Belokurov, V. Evidence for two early accretion events that built the Milky Way stellar halo. *Mon. Not. R. Astron. Soc.* **488**, 1235–1247 (2019).
14. Naidu, R. P. et al. Evidence from the H3 survey that the stellar halo is entirely comprised of substructure. *Astrophys. J.* **901**, 48 (2020).
15. Ruiz-Lara, T., Helmi, A., Gallart, C., Surot, F. & Cassisi, S. Unveiling the past evolution of the progenitor of the Helmi streams. *Astron. Astrophys.* **668**, L10 (2022).
16. Horta, D. et al. The proto-galaxy of Milky Way-mass haloes in the FIRE simulations. *Mon. Not. R. Astron. Soc.* **527**, 9810–9825 (2024).
17. Santistevan, I. B. et al. The formation times and building blocks of Milky Way-mass galaxies in the FIRE simulations. *Mon. Not. R. Astron. Soc.* **497**, 747–764 (2020).
18. Orkney, M. D. A. et al. The impact of two massive early accretion events in a Milky Way-like galaxy: repercussions for the buildup of the stellar disc and halo. *Mon. Not. R. Astron. Soc.* **517**, L138–L142 (2022).
19. García-Bethencourt, G., Brook, C. B., Grand, R. J. J. & Kawata, D. A high fidelity Milky Way simulation with Kraken, Gaia-Enceladus, and Sequoia analogues: clues to their accretion histories. *Mon. Not. R. Astron. Soc.* **526**, 1190–1197 (2023).
20. Woudenberg, H. C. & Helmi, A. The chaos induced by the Galactic bar on the orbits of nearby halo stars. *Astron. Astrophys.* **700**, A240 (2025).
21. Belokurov, V. & Kravtsov, A. From dawn till disc: Milky Way's turbulent youth revealed by the APOGEE+Gaia data. *Mon. Not. R. Astron. Soc.* **514**, 689–714 (2022).
22. Chandra, V. et al. The three-phase evolution of the Milky Way. *Astrophys. J.* **972**, 112 (2024).
23. Malhan, K. & Rix, H.-W. Shiva and Shakti: presumed proto-galactic fragments in the inner Milky Way. *Astrophys. J.* **964**, 104 (2024).
24. Horta, D. & Schiavon, R. P. Modelling the density and mass of the Milky Way's proto-galaxy components with APOGEE-Gaia. *Mon. Not. R. Astron. Soc.* **537**, 3730–3745 (2025).
25. Rix, H.-W. et al. The poor old heart of the Milky Way. *Astrophys. J.* **941**, 45 (2022).
26. Massari, D., Koppelman, H. H. & Helmi, A. Origin of the system of globular clusters in the Milky Way. *Astron. Astrophys.* **630**, L4 (2019).
27. Kruijssen, J. M. D. et al. Kraken reveals itself - the merger history of the Milky Way reconstructed with the E-MOSAICS simulations. *Mon. Not. R. Astron. Soc.* **498**, 2472–2491 (2020).
28. Kruijssen, J. M. D., Pfeffer, J. L., Reina-Campos, M., Crain, R. A. & Bastian, N. The formation and assembly history of the Milky Way revealed by its globular cluster population. *Mon. Not. R. Astron. Soc.* **486**, 3180–3202 (2019).
29. Belokurov, V. & Kravtsov, A. In-situ versus accreted Milky Way globular clusters: a new classification method and implications for cluster formation. *Mon. Not. R. Astron. Soc.* **528**, 3198–3216 (2024).
30. Chen, Y. & Gnedin, O. Y. Galaxy assembly revealed by globular clusters. *Open J. Astrophys.* **7**, 23 (2024).
31. Horta, D. et al. Evidence from APOGEE for the presence of a major building block of the halo buried in the inner Galaxy. *Mon. Not. R. Astron. Soc.* **500**, 1385–1403 (2021).
32. Vasini, A., Spitoni, E. & Matteucci, F. Galactic archaeology with [Mg/Mn] versus [Al/Fe] abundance ratios. Uncertainties and caveats. *Astron. Astrophys.* **683**, A121 (2024).
33. Rix, H.-W. et al. The extremely metal-rich knot of stars at the heart of the Galaxy. *Astrophys. J.* **975**, 293 (2024).
34. Massari, D. et al. Cluster Ages to Reconstruct the Milky Way Assembly (CARMA). I. The final word on the origin of NGC 6388 and NGC 6441. *Astron. Astrophys.* **680**, A20 (2023).
35. VandenBerg, D. A., Brogaard, K., Leaman, R. & Casagrande, L. The ages of 55 globular clusters as determined using an improved ΔV_{TO}^{HB} method along with color-magnitude diagram constraints, and their implications for broader issues. *Astrophys. J.* **775**, 134 (2013).
36. Pfeffer, J. L. et al. Predicting accreted satellite galaxy masses and accretion redshifts based on globular cluster orbits in the E-MOSAICS simulations. *Mon. Not. R. Astron. Soc.* **499**, 4863–4875 (2020).
37. Callingham, T. M. et al. The chemo-dynamical groups of Galactic globular clusters. *Mon. Not. R. Astron. Soc.* **513**, 4107–4129 (2022).
38. Aguado-Agelet, F. et al. Cluster Ages to Reconstruct the Milky Way Assembly (CARMA). II. The age-metallicity relation of Gaia–Sausage–Enceladus globular clusters. *Astron. Astrophys.* **704**, A255 (2025).
39. Ceccarelli, E. et al. Cluster Ages to Reconstruct the Milky Way Assembly (CARMA). III. NGC 288 as the first splashed globular cluster. *Astron. Astrophys.* **704**, A256 (2025).
40. Massari, D. et al. The Hubble Missing Globular Cluster Survey: I. Survey overview and the first precise age estimate for ESO452-11 and 2MASS-GC01. *Astron. Astrophys.* **698**, A197 (2025).
41. Massari, D. Origin of the system of globular clusters in the Milky Way—Gaia eDR3 edition. *Res. Not. Am. Astron. Soc.* **9**, 64 (2025).

42. Speagle, J. S. DYNESTY: a dynamic nested sampling package for estimating Bayesian posteriors and evidences. *Mon. Not. R. Astron. Soc.* **493**, 3132–3158 (2020).
43. Prantzos, N. The metallicity distribution of the halo and the satellites of the Milky Way in the hierarchical merging paradigm. *Astron. Astrophys.* **489**, 525–532 (2008).
44. McMillan, P. J. The mass distribution and gravitational potential of the Milky Way. *Mon. Not. R. Astron. Soc.* **465**, 76–94 (2017).
45. Jeffreys, H. *Theory of Probability.* Oxford Classic Texts in the Physical Sciences (Oxford Univ. Press, 1939).
46. Kass, R. E. & Raftery, A. E. Bayes factors. *J. Am. Stat. Assoc.* **90**, 773–795 (1995).
47. Dekel, A. & Woo, J. Feedback and the fundamental line of low-luminosity low-surface-brightness/dwarf galaxies. *Mon. Not. R. Astron. Soc.* **344**, 1131–1144 (2003).
48. Fernández-Alvar, E. et al. Chronology of our Galaxy from Gaia colour-magnitude diagram fitting (ChronoGal): II. Unveiling the formation and evolution of the kinematically selected thick and thin discs. *Astron. Astrophys.* **704**, A258 (2025).
49. Brodie, J. P. & Strader, J. Extragalactic globular clusters and galaxy formation. *Annu. Rev. Astron. Astrophys.* **44**, 193–267 (2006).
50. Savaglio, S. et al. The Gemini Deep Deep Survey. VII. The redshift evolution of the mass-metallicity relation. *Astrophys. J.* **635**, 260–279 (2005).
51. Robertson, B., Bullock, J. S., Font, A. S., Johnston, K. V. & Hernquist, L. Λ cold dark matter, stellar feedback, and the galactic halo abundance pattern. *Astrophys. J.* **632**, 872–881 (2005).
52. Grand, R. J. J. et al. Overview and public data release of the augmented Auriga Project: cosmological simulations of dwarf and Milky Way-mass galaxies. *Mon. Not. R. Astron. Soc.* **532**, 1814–1831 (2024).
53. Rauer, H. et al. The PLATO mission. *Exp. Astron.* **59**, 26 (2025).
54. Niederhofer, F. et al. Cluster Ages to Reconstruct the Milky Way Assembly (CARMA). IV. Chrono-dynamics of seven old star clusters in the Large Magellanic Cloud and the peculiar origin of NGC 1841. *Astron. Astrophys.* **704**, A257 (2025).
55. Milone, A. et al. The ACS survey of Galactic globular clusters. XII. Photometric binaries along the main sequence. *Astron. Astrophys.* **540**, A16 (2012).
56. Nardiello, D. et al. The Hubble Space Telescope UV Legacy Survey of Galactic Globular Clusters – XVII. Public catalogue release. *Mon. Not. R. Astron. Soc.* **481**, 3382–3393 (2012).
57. Pietrinferni, A. et al. The updated BaSTI stellar evolution models and isochrones – IV. α-depleted calculations. *Mon. Not. R. Astron. Soc.* **527**, 2065–2070 (2024).
58. Hidalgo, S. L. et al. The updated BaSTI stellar evolution models and isochrones. I. Solar-scaled calculations. *Astrophys. J.* **856**, 125 (2018).
59. Piotto, G. et al. The Hubble Space Telescope UV Legacy Survey of Galactic Globular Clusters. I. Overview of the project and detection of multiple stellar populations. *Astron. J.* **149**, 91 (2015).
60. Cohen, R. E. et al. Relative ages of nine inner Milky Way globular clusters from proper motion cleaned color-magnitude diagrams. *Astron. J.* **162**, 228 (2021).
61. Bellini, A. et al. New Hubble Space Telescope WFC3/UVIS observations augment the stellar-population complexity of ω Centauri. *Astron. J.* **140**, 631 (2010).
62. Harris, W. E. A catalog of parameters for globular clusters in the Milky Way. *Astron. J.* **112**, 1487 (1996).
63. Baumgardt, H. Accurate distances to Galactic globular clusters through a combination of Gaia EDR3, HST, and literature data. *Mon. Not. R. Astron. Soc.* **505**, 5957–5977 (2021).
64. Salaris, M., Chieffi, A. & Straniero, O. The alpha-enhanced isochrones and their impact on the FITS to the Galactic globular cluster system. *Astrophys. J.* **414**, 580 (1993).
65. Chaboyer, B. et al. An accurate relative age estimator for globular clusters. *Mon. Not. R. Astron. Soc.* **283**, 683 (1996).
66. Marin-Franch, A. et al. The ACS Survey of Galactic globular clusters. VII. Relative ages. *Astrophys. J.* **694**, 1498 (2009).
67. Dotter, A. et al. The ACS Survey of Galactic globular clusters. IX. Horizontal branch morphology and the second parameter phenomenon. *Astrophys. J.* **708**, 698 (2010).
68. Hughes, M. E. et al. Fossil stellar streams and their globular cluster populations in the E-MOSAICS simulations. *Mon. Not. R. Astron. Soc.* **482**, 2795–2806 (2019).
69. Carretta, E. & Bragaglia, A. The in situ origin of the globular cluster NGC 6388 from abundances of Sc, V, and Zn of a large sample of stars. *Astron. Astrophys.* **660**, 1 (2022).

Acknowledgements

This paper should be considered as one of the contributions to the CARMA series of papers. This work presents results from the European Space Agency (ESA) space mission Gaia. Gaia data are being processed by the Gaia Data Processing and Analysis Consortium (DPAC). Funding for the DPAC is provided by national institutions, in particular the institutions participating in the Gaia MultiLateral Agreement (MLA). Based on observations with the NASA/ESA HST, obtained at the Space Telescope Science Institute, which is operated by AURA, Inc., under NASA contract NAS 5-26555. S.C., M.M., C.G., E.P., S.S., M.S. and A.M. are core members of the CARMA project and contributed decsively to the development of the CARMA framework.

Author contributions

D.M. coordinated the project and led the scientific interpretation. C.Z. performed the photometric analysis and the isochrone fitting. C.F. led the statistical analysis of the results. A.H. critically contributed to the interpretation of the results and to the writing of the manuscript. E.C. contributed to the photometric analysis. F.A.-A. developed the isochrone fitting code. A.B. produced the photometry of NGC 4372. R.E.C. provided the photometric catalogues of NGC 6401, NGC 6254 and NGC 6256. T.M.C. and E.W. provided the analysis of cosmological simulations and contributed to the statistical analysis. H.C.W. performed the GC orbital integration in a barred gravitational potential. S.C., M.M., C.G., E.P., S.S., M.S. and A.M. contributed decisively to the development of the CARMA framework.

Funding

D.M., S.C. and E.P. acknowledge financial support from PRIN-MIUR-22: 'CHRONOS: adjusting the clock(s) to unveil the CHRONO-chemo-dynamical Structure of the Galaxy' (PI, S.C.). D.M. acknowledges financial support from the Italian Ministry of University and Research (grant FIS2023 – 01611, CUP C53C25000300001) and from the INAF Mini-Grant 1.05.24.07.02. C.F. acknowledges support from the PRIN INAF 2023 grant ObFu N^2RED (PI, C.F.). C.G. and S.C. acknowledge support from the Agencia Estatal de Investigación del Ministerio de Ciencia e Innovación (AEI-MCINN) under grant 'At the forefront of Galactic Archaeology: evolution of the luminous and dark matter components of the Milky Way and Local Group dwarf galaxies in the Gaia era' with references PID2020-118778GB-I00/10.13039/501100011033 and PID2023-150319NB-C21/C22/10.13039/501100011033. C.G. also acknowledges support from the Severo Ochoa programme through CEX2019-000920-S. M.M. acknowledges support from the Agencia Estatal de Investigación del Ministerio de Ciencia e Innovación (MCIN/AEI) under the grant 'RR Lyrae stars, a lighthouse to distant galaxies and early galaxy evolution' and the European Regional Development Fun (ERDF) with reference

PID2021-127042OB-I00. A.H., T.M.C., E.W. and H.C.W. acknowledge financial support from a Spinoza Award from NWO (SPI 78-411). Co-funded by the European Union (ERC-2022-AdG, 'StarDance: the non-canonical evolution of stars in clusters', grant agreement 101093572, PI, E.P.). Open access funding provided by Istituto Nazionale di Astrofisica within the CRUI-CARE Agreement.

Competing interests
The authors declare no competing interests.

Additional information
Supplementary information The online version contains supplementary material available at https://doi.org/10.1038/s41550-026-02931-5.

Correspondence and requests for materials should be addressed to Davide Massari.

Peer review information *Nature Astronomy* thanks Diederik Kruijssen and the other, anonymous, reviewer(s) for their contribution to the peer review of this work.

[1]Osservatorio di Astrofisica e Scienza dello Spazio di Bologna, INAF, Bologna, Italy. [2]Dipartimento di Fisica e Astronomia, Università degli Studi di Bologna, Bologna, Italy. [3]Kapteyn Astronomical Institute, University of Groningen, Groningen, The Netherlands. [4]Escola de Enxeñaría de Telecomunicación, Universidade de Vigo, Vigo, Spain. [5]Universidad de La Laguna, La Laguna, Spain. [6]Osservatorio Astronomico di Abruzzo, INAF, Teramo, Italy. [7]Sezione di Pisa, INFN, Universitá di Pisa, Pisa, Italy. [8]LIRA, Observatoire de Paris, Université PSL, Sorbonne Université, Université Paris Cité, CY Cergy Paris Université, Meudon, France. [9]Osservatorio Astronomico di Roma, INAF, Monte Porzio Catone, Italy. [10]Space Telescope Science Institute, Baltimore, MD, USA. [11]Institute for Astronomy, University of Edinburgh, Royal Observatory, Edinburgh, UK. [12]Department of Physics and Astronomy, Rutgers the State University of New Jersey, Piscataway, NJ, USA. [13]Instituto de Astrofísica de Canarias, La Laguna, Spain. [14]Osservatorio Astrofisico di Arcetri, INAF, Firenze, Italy. [15]Astrophysics Research Institute, Liverpool John Moores University, Liverpool, UK. ✉e-mail: davide.massari@inaf.it